JACS
JOURNAL OF THE AMERICAN CHEMICAL SOCIETY
Article
pubs.acs.org/JACS

Photoelectron Spectroscopy of the Methide Anion: Electron Affinities of $^{\bullet}CH_3$ and $^{\bullet}CD_3$ and Inversion Splittings of CH_3^- and CD_3^-

Allan M. Oliveira,[†,‡] Yu-Ju Lu,[†,‡,⊥] Julia H. Lehman,[†,‡] P. Bryan Changala,[†,§] Joshua H. Baraban,[‡,∥] John F. Stanton,[∥] and W. Carl Lineberger*[,†,‡]

[†]JILA, [‡]Department of Chemistry and Biochemistry, and [§]Department of Physics, University of Colorado, Boulder, Colorado 80309, United States

[∥]Department of Chemistry, University of Texas, Austin, Texas 78712, United States

Supporting Information

ABSTRACT: We report high-resolution photoelectron spectra of the simplest carbanions, CH_3^- and CD_3^-. The vibrationally resolved spectra are dominated by a long progression in the umbrella mode (ν_2) of $^{\bullet}CH_3$ and $^{\bullet}CD_3$, indicating a transition from a pyramidal C_{3v} anion to the planar D_{3h} methyl radical. Analysis of the spectra provides electron affinities of $^{\bullet}CH_3$ (0.093(3) eV) and $^{\bullet}CD_3$ (0.082(4) eV). These results enable improved determination of the corresponding gas-phase acidities: $\Delta_{acid}H_{0K}^{\circ}(CH_4)$ = 414.79(6) kcal/mol and $\Delta_{acid}H_{0K}^{\circ}(CD_4)$ = 417.58(8) kcal/mol. On the basis of the photoelectron anisotropy distribution, the electron is photodetached from an orbital with predominant p-character, consistent with the sp^3-hybridized orbital picture of the pyramidal anion. The double-well potential energy surface along the umbrella inversion coordinate leads to a splitting of the vibrational energy levels of the umbrella mode. The inversion splittings of CH_3^- and CD_3^- are 21(5) and 6(4) cm^{-1}, respectively, and the corresponding anion umbrella vibrational frequencies are 444(13) and 373(12) cm^{-1}, respectively. Quantum mechanical calculations reported herein show good agreement with the experimental data and provide insight regarding the electronic potential energy surface of CH_3^-.

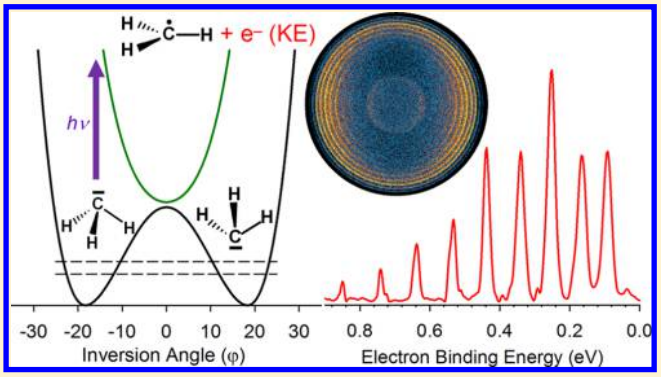

1. INTRODUCTION

Carbanions, anions with a formal negative charge located at a carbon center, are ubiquitous in many areas of chemistry.[1] In solution, carbanions are an integral part of the mechanism for carbon−carbon bond formation in organic synthesis and carbon−metal bonds in inorganic chemistry.[2] Carbanion chemistry has also been applied in biochemistry,[3,4] such as through carbanion-mediated mechanisms of photodecaging in photoremoveable protecting groups.[5] While typically stabilized by counterions in solution, isolated gas-phase carbanions have also been the focus of many experimental and theoretical studies to gain insight into their reactivity and chemical structure.[4,6] The methide anion (CH_3^-), which is predicted to be in Titan's atmosphere,[7−10] is the simplest carbanion and is the focus of this study.

The first gas-phase experimental observation of methide by Ellison et al.[11] resulted in the determination of the electron affinity (EA) of the methyl radical as 0.08 ± 0.03 eV via negative ion photoelectron spectroscopy. From this measurement, the gas-phase acidity ($\Delta_{acid}H_{0K}^{\circ}$) was derived for CH_4 as 415.2(7) kcal/mol. Methane has one of the highest observed gas-phase acidities,[12,13] second only to LiOH.[14] DePuy et al. used the CH_4 gas-phase acidity, or deprotonation enthalpy, as a reference point to determine other alkane acidities.[13] It is this large gas-phase acidity of methane, or the high reactivity of CH_3^-, that has made this carbanion challenging to produce and stabilize, so relatively few experimental studies of isolated CH_3^- exist.[15,16]

The neutral methyl radical, on the other hand, has received extensive theoretical and experimental attention[17−29] in part due to its importance as a combustion intermediate. High-resolution rovibrational spectroscopic studies have determined the vibrational frequencies and rotational constants to high (subwavenumber) precision.[21−23] These experiments, together with high-level calculations,[25,30,31] confirmed that the $^{\bullet}CH_3$ radical is a trigonal planar molecule with D_{3h} symmetry.

The low-resolution CH_3^- photoelectron spectrum reported by Ellison et al. exhibited a long vibrational progression in the ν_2 umbrella mode of the $\tilde{X}\ ^2A''$ ground state of $^{\bullet}CH_3$, indicating transitions from a pyramidal anion of C_{3v} symmetry to the planar D_{3h} $^{\bullet}CH_3$. The pyramidal structure of CH_3^- results in a double-well electronic potential energy surface along the inversion coordinate, which leads to a splitting of vibrational levels below the barrier to inversion. The magnitude of the splitting (Δ_{inv}) depends on the barrier size with respect to the

Received: July 6, 2015
Published: September 21, 2015

DOI: 10.1021/jacs.5b07013
J. Am. Chem. Soc. 2015, 137, 12939−12945

vibrational levels of the system. The inversion splitting has been well-characterized in the isoelectronic NH_3 and H_3O^+ species. Because of the numerous experimental and theoretical studies available for these molecules, both have become prototypes in studying inversion splitting, as well as tests for the validity of new theoretical treatments. In NH_3,[32−34] the inversion splitting of the ground vibrational state, the transition employed in the first MASER (microwave amplification by stimulated emission of radiation),[35] has been experimentally determined as 0.793 cm^{-1} (24 GHz);[32,36] for hydronium, H_3O^+, a smaller inversion barrier leads to a much larger splitting of 55.35 cm^{-1}.[37−39] Isotopic substitution, i.e., ND_3 and D_3O^+, lowers the inversion splitting to 0.053 and 15.36 cm^{-1}, respectively.[34,39] The inversion splittings of CH_3^- and its isotopologue, CD_3^-, however, have not been experimentally determined prior to the present study.

There has been considerable theoretical attention directed toward the CH_3^- anion,[31,40−47] in particular to the calculation of the inversion splitting, which is predicted to be on the order of 20 cm^{-1}.[44,47] Calculated structures are consistent with the experimentally determined pyramidal geometry.[11] However, calculations have resulted in a range of EAs, depending on the level of theory and basis set used.[22,47] The strong anharmonicity of the anion electronic potential surface complicates the calculation of both the vibrational zero-point energy (ZPE) and the effective inversion barrier size. According to previous theoretical work, the change in ZPE between the anion and the neutral (ΔZPE) in this system accounts for at least 50% of the EA.[48] The ZPE in combination with the barrier shape has a large effect on the magnitude of the inversion splitting, and therefore, a very high quality surface is required for reliable calculations. An experimental measurement of the inversion splitting and vibrational frequencies of the anion are essential to accurately evaluate the calculated CH_3^- potential energy surfaces.

In the present work, we report high-resolution photoelectron spectra of CH_3^-, resulting in the determination of more accurate values of the $^{\bullet}CH_3$ electron affinity, anion umbrella mode vibrational frequency, and gas-phase acidity of CH_4. These experimental parameters are obtained for the fully deuterated species for the first time. The photoelectron angular distribution serves as a direct probe of the CH_3^- HOMO, resulting in an experimental measurement of its relative p-type orbital character, agreeing with the sp^3 orbital hybridization picture. We also report the first experimental determination of the ground-state inversion splitting of these simplest carbanions. The experimental results provide a point of reference for building an accurate potential energy surface for the methide anion. New high-level electronic structure and vibrational calculations of the CH_3^- and CD_3^- anions show excellent agreement with experimental findings.

2. EXPERIMENTAL METHODS

The experiments employ a negative ion photoelectron velocity-map imaging (VMI) spectrometer described previously.[49] Briefly, ions are generated in a novel pulsed plasma-entrainment anion source described in detail elsewhere.[50] This anion source consists of two perpendicularly oriented general valves: the main valve (40 psig of argon) and side valve (20 psig of CH_4, 99.99% purity, or CD_4, 99% atom D), where the low-flow side valve generates ions in a plasma formed in a pulsed electrical discharge (−900 V, 40−100 μs). The plasma is then entrained into the argon gas expansion from the main valve, which provides collisional cooling/stabilization. Downstream of the main expansion, the anions are extracted into a Wiley−McLaren time-of-flight (TOF) mass spectrometer, where they are accelerated, steered, separated by their mass-to-charge (m/z) ratio, and spatially focused onto an inline microchannel plate (MCP) detector. Prior to the inline detector, an appropriately timed laser pulse spatially and temporally overlaps the desired anions; the photodetached electrons, are perpendicularly extracted by a pulsed electric field, constituting the first stage of a VMI photoelectron spectrometer. The VMI spectrometer provides a 2D projection of the 3D velocity-mapped electrons onto an MCP/phosphor-coupled charge-coupled device (CCD) camera detector. The primary experimental observables are the photoelectron velocity and angular distributions resulting from photodetachment of an electron from the HOMO of mass-selected CH_3^- and CD_3^- anions. The photoelectron images, shown in Figures 1 and 2, are then converted to kinetic energy distributions following inverse Abel transformation through the BASEX algorithm[51] and Jacobian transform, yielding the reported photoelectron spectra.

We employ two different photon energies to obtain the photoelectron spectra: the fundamental output of a Nd:YAG laser (1064 nm, 1.165 eV) and 3239 nm (0.383 eV). This mid-IR wavelength comes from difference frequency generation (DFG) of 1064 nm with 801 nm (532 nm pumped LDS 798 dye laser) in a 1 × 1 × 3 cm^3 magnesium oxide-doped lithium niobate crystal ($MgO:LiNbO_3$). The 1064 nm light (3.5 mJ/pulse) or the mid-IR light (50−100 μJ/pulse) is focused into the interaction region using a 0.5 m focal length CaF_2 lens. The dye laser wavelengths are measured using a He−Ne laser calibrated wavemeter (Atos MK Photonics) to calculate the mid-IR wavelength. All wavelengths are vacuum corrected.

The photoelectron spectra are reported as a function of the electron binding energy (eBE = $h\nu$ − eKE, where eKE = electron kinetic energy), a quantity that is independent of the laser wavelength used for photodetachment. The energy scale is calibrated by using the ν_2 umbrella mode frequencies in $^{\bullet}CH_3$ and $^{\bullet}CD_3$, experimentally determined from high-resolution IR absorption studies.[21,23] We further verified the accuracy of the energy scale by using an external calibration. Here, the kinetic energy scale is determined by the vibrational level spacing in the O_2^- photoelectron spectrum. The values and error bars reported herein are weighted averages of all measurements, which include the uncertainty in the energy-scale calibration, statistical error in the peak center given by a least-squares Gaussian fit to the experimental peaks, and error associated with a displacement from the peak center due to a rotational band-origin shift (discussed further in the next section). For additional details see the Supporting Information.

3. EXPERIMENTAL RESULTS

The plasma entrainment anion source[50] enables efficient synthesis and cooling of CH_3^-. This method of CH_3^- generation is a significant departure from the commonly employed anion deprotonation chemistry, due to the lack of an anion capable of deprotonating methane. The experimental photoelectron spectra of CH_3^- and CD_3^-, depicted in the top panels of Figures 1 and 2, respectively, show an extended vibrational progression indicative of a large geometry change upon electron photodetachment.

The overall CH_3^- spectrum is consistent with the lower resolution one reported by Ellison et al.[11] The CD_3^- photoelectron spectrum reported here is the only experimental result obtained for this isotopic species. The binding energies corresponding to the center of each labeled peak are shown in Table S1. The small features between peaks C and E are not reproducible and are artifacts from the inverse Abel transformation when converting the photoelectron images to the 1D spectra.

In addition, the high-resolution photoelectron imaging spectra yield photoelectron angular distributions with respect to the laser polarization, giving the anisotropy parameter (β) of the detached electrons.[52] The eKE dependence of β yields

DOI: 10.1021/jacs.5b07013
J. Am. Chem. Soc. 2015, 137, 12939−12945

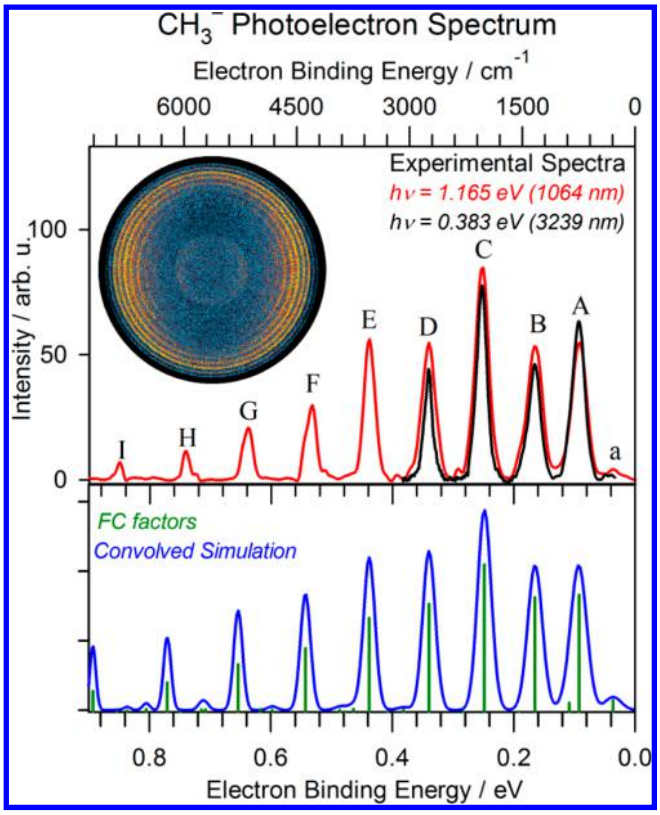

Figure 1. Photoelectron spectra of CH_3^-. The experimental spectra using a 1.165 eV (red) or 0.383 eV (black) photon energy are shown in the upper panel. The peak assignments (upper- and lowercase letters) and positions are provided in Table S1. The inset shows a raw velocity-mapped photoelectron image using a 1.165 eV photon energy, with the direction of the laser polarization parallel to the *y*-axis of the graph. Note that the center ring in the image is a contaminant due to detachment from CH_2^-. The lower panel shows the spectrum calculated by methods described in section 4.2.

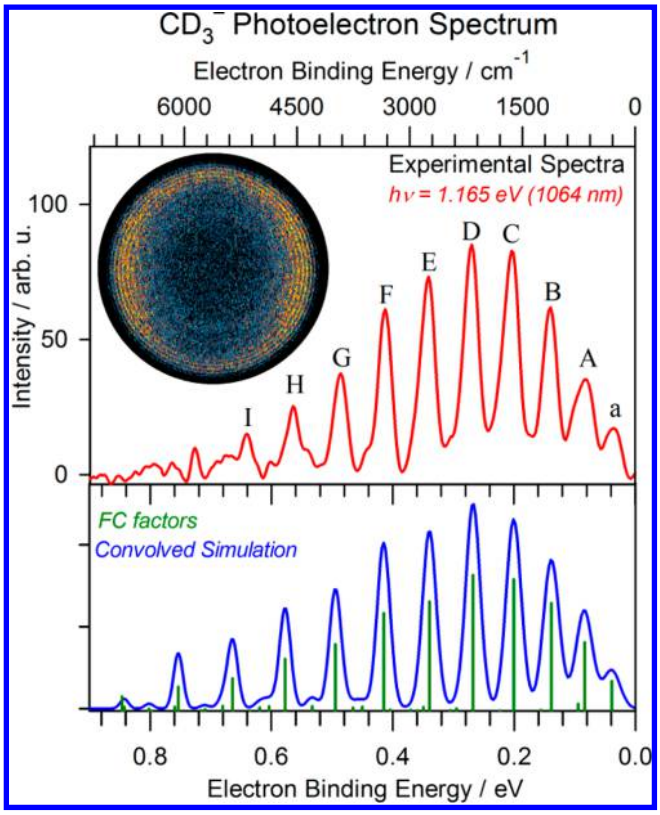

Figure 2. Photoelectron spectra of CD_3^-. Description analogous to that of Figure 1.

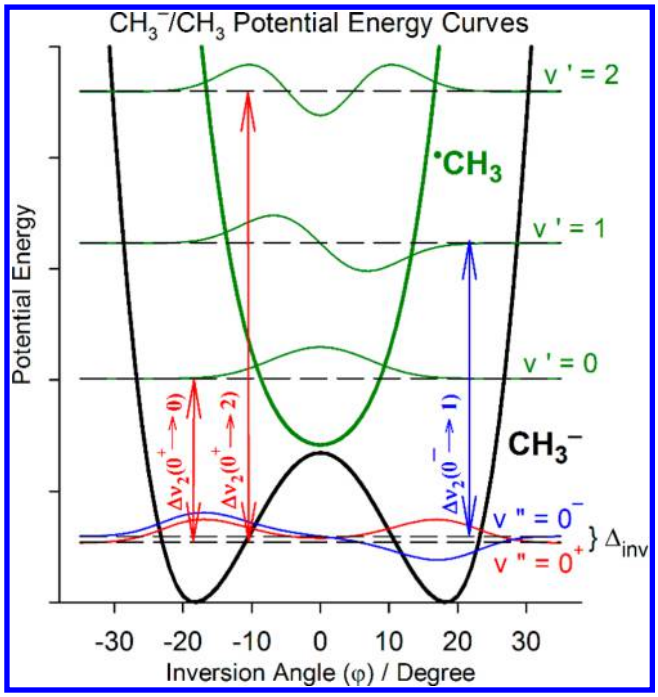

Figure 3. Schematic potential energy curves (not to scale) of CH_3^- (black) and $^{\bullet}CH_3$ (green) as a function of the inversion angle (ϕ). The red and blue arrows indicate the nonzero Franck–Condon factors from $v'' = 0^+$ (even wave function in red) and $v' = 0^-$ (odd wave function in blue) in the anion ground state to even and odd quanta of the neutral state, respectively. The inversion splitting in the anion state is labeled Δ_{inv}. See the text for details.

direct information about the hybrid orbital composition of the methide anion highest occupied molecular orbital (HOMO). Photoelectron imaging is a powerful tool for obtaining both molecular orbital energies and their symmetries, as is reviewed in the work of Sanov et al.[53,54] By fitting the anisotropy parameter observed for each of the peaks in the vibrational progression as a function of the electron kinetic energy using the Wigner–Bethe–Cooper–Zare equation, modified for mixed sp states (see Figure S1),[55,56] we find that the kinetic energy dependence is indicative of electron photodetachment from an orbital that has a predominant p component (0.80 p fraction; see the Supporting Information) as indicated by Figure S1 and Table S3. This new experimental observable is evidence for the detached electron originating from a carbon atom hybrid sp^3 orbital in the pyramidal CH_3^-, in agreement with the expected, distorted sp^3 hybridization for CH_3^-. An expansion of the HOMO of CH_3^- from the calculated structure as a linear combination of hydrogenic s and p orbitals yields a p fraction of 0.89, consistent with the experimental value. Additional fit parameters and sensitivities, including discussion of the diffuse orbital nature of the CH_3^- HOMO, can be found in the Supporting Information.

Because of the anion double-well potential energy surface along the umbrella inversion coordinate (see Figure 3), the ground vibrational state is split into two levels of opposite parity with respect to the umbrella inversion. These inversion

DOI: 10.1021/jacs.5b07013
J. Am. Chem. Soc. 2015, 137, 12939–12945

levels are labeled as 0^+, the lower, even parity inversion level, and 0^-, the upper, odd parity inversion level. Figure 3 shows a schematic 1D representation (not to scale) of the potential energy surfaces of CH_3^- (black) and $^\bullet CH_3$ (green) as a function of the umbrella inversion angle (ϕ), where $\phi = 0°$ represents the D_{3h} symmetry planar structure.

The anion and neutral potential energy curves were calculated by the methods described in section 4 and are the relaxed inversion potential for the anion, where at each value of ϕ the C−H bond lengths are optimized. The wave functions shown in Figure 3 were calculated numerically using the Numerov method. The symmetries of the wave functions of these levels determine the selection rules in the photoelectron spectrum. The only allowed transitions (i.e., nonvanishing Franck−Condon factors) are from the anion $\nu_2(v'' = 0^+)$ to the neutral $\nu_2(v' = 0, 2, 4, ...)$ and from the anion $\nu_2(v'' = 0^-)$ to the neutral $\nu_2(v' = 1, 3, 5, ...)$. Note that the 1^+ level refers to the lower inversion $\nu_2(v'' = 1)$ level of the anions.

The peaks labeled "A" in both spectra (Figures 1 and 2) correspond to the $\nu_2(v'' = 0^+ \rightarrow v' = 0)$ transition, with centers at 0.094(2) and 0.083(3) eV, respectively. Each vibrational peak, however, is comprised of an unresolved family of rotational transitions, and the peak center need not correspond to the "rotationless" transition. This small shift can be approximately taken into account using a procedure from Engelking,[57] as described in the Supporting Information. This shift results in adiabatic EAs of 0.093(3) and 0.082(4) eV for $^\bullet CH_3$ and $^\bullet CD_3$, respectively. The uncertainties include a contribution due to the estimated 150 ± 50 K anion rotational temperature. This EA($^\bullet CH_3$) is consistent with that of Ellison et al. of 0.08(3) eV, but with an order of magnitude improvement in precision.

The first peak in the each progression, labeled as "a" (Figures 1 and 2), corresponds to a vibrational hot-band transition. The vibrational frequency of the $\nu_2(v'' = 0^+ \rightarrow 1^+)$ umbrella mode in the anion is 444(13) cm^{-1} in CH_3^- and 373(12) cm^{-1} in CD_3^-. The spacing between adjacent peaks in the photoelectron spectra shown in Figures 1 and 2 gives the vibrational frequencies of $^\bullet CH_3$ or $^\bullet CD_3$, respectively. The vibrational frequencies in the neutral state have been measured to very high precision by Yamada et al.[19] ($^\bullet CH_3$) and by Sears et al.[23] ($^\bullet CD_3$) using diode-laser IR absorption spectroscopy.[21,23] Because of the aforementioned vibrational selection rules, however, the peaks in the photoelectron spectra are irregularly spaced compared to the neutral umbrella mode frequencies. Specifically, the transitions to the odd vibrational quanta in the neutral are red-shifted (to lower electron binding energy) by Δ_{inv}, as Figure 3 shows. Thus, our measured relative peak-center positions and the high-resolution IR data will not be consistent unless Δ_{inv} is taken into account. The following equation is a sample procedure to obtain the inversion splitting from the experimental data:

$$\Delta_{inv}(CH_3^-, 0^+ \rightarrow 0^-) = \nu_2(^\bullet CH_3, 0 \rightarrow 3) + \mathrm{eBE}[\mathrm{A}(v'' = 0^+ \rightarrow v' = 0)] - \mathrm{eBE}[\mathrm{D}(v'' = 0^- \rightarrow v' = 3)]$$

This equation utilizes the high-resolution measurement[21] of the $^\bullet CH_3$ $\nu_2(0-3)$ levels and our determination of the eBE corresponding to the centers of peaks A and D; the primes and double primes represent ν_2 levels in the neutral and anion states, respectively. The equation is also generalized to the other observed peaks. A weighted least-squares minimization of the difference between the relative peak spacing and the high-resolution data, where Δ_{inv} is the optimization parameter, is used to determine Δ_{inv}. With this procedure, all measured frequencies are used in the determination of Δ_{inv}. This procedure results in Δ_{inv} values of 21(5) cm^{-1} in CH_3^- and 6(4) cm^{-1} in CD_3^-. The largest contribution to the reported uncertainties in the inversion splittings is due to the relative shift in the rotational band origin with increasing vibrational quanta, which is on the order of 4 cm^{-1}; see the Supporting Information for additional details.

The neutral $^\bullet CH_3/^\bullet CD_3$ vibrational frequencies are shown in Table S2. These new data provide seven additional vibrational levels of the methyl radical, namely, $\nu_2(6-8)$ in $^\bullet CH_3$ and $\nu_2(5-8)$ in $^\bullet CD_3$. A quadratic fit of the vibrational level spacings as a function of the vibrational quantum number results in vibrational constants $\omega_2(^\bullet CH_3) \approx 627$ cm^{-1}, $x_{22}(^\bullet CH_3) \approx 18$ cm^{-1}, $\omega_2(^\bullet CD_3) \approx 474$ cm^{-1}, and $x_{22}(^\bullet CD_3) \approx 11$ cm^{-1}, with deviations that fall within the error bars (see Table S2). Experimentally determined properties of the anion and neutral, together with the theoretical results, are summarized in Table 1.

Table 1. Summary of Major Results

	Experiment	Calculation
EA($^\bullet CH_3$)	0.093(3) eV	0.094 eV
$\Delta_{inv}(CH_3^-, \nu_2(0^+ \rightarrow 0^-))$	21(5) cm^{-1}	25.0 cm^{-1}
CH_3^- $\nu_2(0^+ \rightarrow 1^+)$	444(13) cm^{-1}	412.3 cm^{-1}
$\Delta_{acid}H_{0K}°(CH_4)$	414.79(6) kcal/mol	
$\Delta_{acid}H_{298K}°(CH_4)$	416.4(2) kcal/mol	
EA($^\bullet CD_3$)	0.082(4) eV	0.084 eV
$\Delta_{inv}(CD_3^-, \nu_2(0^+ \rightarrow 0^-))$	6(4) cm^{-1}	7.9 cm^{-1}
CD_3^- $\nu_2(0^+ \rightarrow 1^+)$	373(12) cm^{-1}	335.9 cm^{-1}
$\Delta_{acid}H_{0K}°(CD_4)$	417.58(8) kcal/mol	
$\Delta_{acid}H_{298K}°(CD_4)$	419.2(2) kcal/mol	

4. THEORETICAL METHODS AND RESULTS

4.1. Anion Potential Energy Surface. The calculation of the anion potential energy surface uses a reduced dimension approximation in lieu of a full dimensional treatment. All HCH bond angles are constrained to be equal, thereby enforcing 3-fold symmetry. This leaves the three C−H bond lengths and the umbrella inversion angle ϕ as the four unconstrained degrees of freedom. Test calculations using NH_3 validate this choice of constraints (see the Supporting Information). The 4D potential energy surface was calculated using the CFOUR quantum chemistry package.[58] The $J = 0$ nuclear motion calculations were performed using discrete variable representation (DVR) bases for the four active vibrational degrees of freedom and numerical evaluation of the kinetic energy operator, as implemented in the program NITROGEN.[59] Using methods discussed in the Supporting Information, we obtain a calculated 4D inversion barrier of ca. 400 cm^{-1} for CH_3^-. Additional details of the calculations and vibrational term values for both the CH_3^- and CD_3^- isotopologues are given in the Supporting Information.

The calculated barrier height is further validated through comparison with the experimental results of the inversion splitting and the anion umbrella mode vibrational frequency. To compare the values, we construct a scaled potential surface as described in the Supporting Information. This scaled surface

DOI: 10.1021/jacs.5b07013
J. Am. Chem. Soc. 2015, 137, 12939−12945

is used to calculate the anion umbrella vibrational frequency and inversion splitting. The calculated ground-state inversion splittings for CH_3^- and CD_3^- are 25.0 and 7.9 cm^{-1}, respectively. This is in excellent agreement with our measured values of 21(5) and 6(4) cm^{-1}. The anion $\nu_2(v'' = 0^+ \rightarrow 1^+)$ calculated frequencies are 412.3 and 335.9 cm^{-1} for CH_3^- and CD_3^-, respectively, which are also in reasonably good agreement with the experimental values of 444(13) and 373(12) cm^{-1}.

4.2. Photoelectron Spectra and Electron Affinities. To calculate photoelectron spectra, we determine Franck−Condon factors (FCFs) by direct computation of vibrational overlap integrals between the anion and neutral DVR wave functions. The simulated spectra for CH_3^- and CD_3^- are shown, respectively, in the lower panels of Figures 1 and 2. The Franck−Condon factors (green sticks) were convolved with Gaussians of varying full width at half-maximum (fwhm) that match the experimental resolution (blue trace), where the calculated FCFs are directly proportional to the area of each peak. The calculated spectrum was shifted such that the origin transition coincides with the origin of the experimental spectra. Despite their approximate nature, the simulated spectra match the experimental spectra quite well, with the main Franck−Condon envelope clearly reproduced.

The calculated values of the electronic contribution to the electron affinity, ΔE_{elec}, at the same levels of theory as those used to determine the barrier height correction, ΔTS, are given in Table S5. ΔE_{elec} is the energy difference between the anion and the neutral potential energy minima; comparison with the experimentally measured adiabatic EA requires a determination of the anion and neutral ZPEs, since EA = ΔE_{elec} + Δ(ZPE). Here, we estimate a total ΔE_{elec} of 415 cm^{-1}, or 0.051 eV, around half the measured EA values. Table S7 summarizes the calculated anion and neutral ZPEs, determined by anharmonic VPT2 calculations performed at the CCSD(T)/d-aug-pVTZ level of theory. This yields calculated EAs for $^{\bullet}CH_3$ and $^{\bullet}CD_3$ of 0.094 and 0.084 eV, respectively. We conservatively estimate that the ZPE and electronic contributions to the calculated EA have a total uncertainty of 100 cm^{-1} (ca. 0.010 eV), to which the electronic part is the main contributor. These results, together with the experimental findings, are reported in Table 1.

5. DISCUSSION

5.1. Gas-Phase Acidities. With the more accurately experimentally determined value for EA($^{\bullet}CH_3$) and the new experimental measurement of EA($^{\bullet}CD_3$), we can obtain the gas-phase acidity at 0 K of CH_4 and CD_4. The following equation shows how the gas-phase acidity of CH_4 is obtained through the thermochemical cycle:

$$\Delta_{acid}H_{0K}^{\circ}(CH_4) = D_0(CH_3{-}H) + IE(H) - EA(CH_3)$$

where $D_0(CH_3{-}H)$ is the bond dissociation energy (BDE) of the C−H bond in methane (103.340(16) kcal/mol),[60] IE(H) is the ionization energy of the hydrogen atom (313.59 kcal/mol),[61] and EA($^{\bullet}CH_3$) is 2.14(6) kcal/mol as reported here. An analogous procedure is followed to obtain the $\Delta_{acid}H_{0K}^{\circ}$ of CD_4 using the corresponding $D_0(^{\bullet}CD_3{-}D)$ = 105.80(3) kcal/mol,[62] IE(D) = 313.67 kcal/mol[61] (IP = ionization potential), and EA($^{\bullet}CD_3$) = 1.90(8) kcal/mol. We obtain gas-phase acidities $\Delta_{acid}H_{0K}^{\circ}(CH_4)$ = 414.79(6) kcal/mol and $\Delta_{acid}H_{0K}^{\circ}(^{\bullet}CD_4)$ = 417.57(8) kcal/mol. Compared to the previously determined value for CH_4 of 415.2(7) kcal/mol, this new value is consistent but with an order of magnitude improvement in precision, a consequence of the better determined electron affinities. We also determine the gas-phase acidities at 298 K, as described by Ervin et al.[63] Here, we rely on the measured vibrational frequencies (with inversion levels) when available and the calculated values otherwise (Table S6), which include the rotational constants for the anion (see the Supporting Information for more details). This leads to $\Delta_{acid}H_{298K}^{\circ}(CH_4)$ = 416.4(2) kcal/mol, also in agreement with Ervin et al.'s value of 416.8(7) kcal/mol, and $\Delta_{acid}H_{298K}^{\circ}(CD_4)$ = 419.2(2) kcal/mol.

5.2. Inversion Splitting, Electron Affinity, and Anion Potential Energy Surface. The inversion splittings of isoelectronic species NH_3 and H_3O^+ and their isotopologues have been determined previously to very high precision. The corresponding experimental values are 0.793 and 0.053 cm^{-1} for NH_3 and ND_3 and 55.35 and 15.36 cm^{-1} for H_3O^+ and D_3O^+, respectively.[32−34,37,38] One of the most valuable results theoretical calculations can give us is the barrier to inversion, since it is not an experimentally measurable quantity. In previous work, Rajamäki et al.[48,64] conducted high-level 6D potential energy surface calculations of NH_3 and H_3O^+ and their isotopologues, comparing the calculated vibrational frequencies of the umbrella mode and inversion splittings with the experimental data. They achieved subwavenumber accuracy for the inversion splittings and reported the associated calculated barrier height as 650 cm^{-1} for H_3O^+ and 1782 cm^{-1} for NH_3. However, the CH_3^- system presents a larger challenge for accurate theoretical treatment of the potential energy curve compared to NH_3 or H_3O^+ since neither of these simpler species present the possibility of electron autodetachment at planarity.

With this measurement of Δ_{inv} and the fundamental anion ν_2 frequency, some of the most important parameters to accurately map out the potential energy surface of the anion are now known. The calculations reported herein reproduce the experimental spectra very well but, most importantly, reproduce the Δ_{inv} and the fundamental ν_2 frequency $(v'' = 0^+ \rightarrow 1^+)$ of the anion umbrella mode. This gives us confidence in our effective barrier to inversion. Note that in section 4 we report a 4D inversion barrier of ca. 400 cm^{-1}, which includes the ZPE of the degenerate bending mode. The effective 1D barrier height (E_B^{eff}), on the other hand, includes the zero-point contributions from the remaining stretching vibrational modes (which differ substantially between the pyramidal and planar geometries, indicating a strong cross-anharmonicity between the inversion motion and the CH stretches), resulting in an effective 1D barrier of 661 cm^{-1}. Our effective 1D barrier is reasonably close to that found by Kraemer et al.[47] (ca. 833 cm^{-1}), and the tunneling splittings calculated in their work are similar to ours (25.0 and 7.9 for CH_3^- and CD_3^-, respectively, from the present calculations versus 19 and 4 cm^{-1} in ref 47.). However, it should be emphasized here that our tunneling calculations are based on a multidimensional model, and a focus on 1D barriers and their dynamics can be misleading. For example, work by Rajamäki et al.[48,64] indicates that the 1D effective barrier for the hydronium ion inversion is comparable to that calculated here for methide, but the magnitude of the tunneling splitting is significantly greater in the former (55 cm^{-1} versus 21 cm^{-1}). While this is surprising at first, the anharmonicities associated with inversion are greater in methide than in hydronium, which is ultimately responsible for the quite different tunneling

DOI: 10.1021/jacs.5b07013
J. Am. Chem. Soc. 2015, 137, 12939−12945

splittings, underscoring the sensitivity of this quantity to details of the multidimensional potential surface.

The most recent theoretical work by Dixon et al.,[44] at the CCSD(T) level of theory with aug-cc-pVxZ (x = D, T, Q) basis sets, found that the stability of the anion increases with the size of the basis set used. From a complete basis set extrapolation, they predicted a best-estimate adiabatic EA of 0.07(1) eV, which is in relatively good agreement with the experimentally determined value. They report that 63% of the EA comes from ΔZPE contributions between the anion and neutral species and that most of their uncertainty comes from the calculation of the anion ZPE. However, the calculated fundamental vibrational frequencies of the ν_2 mode were reported as 783.8 cm^{-1} for CH_3^- and 496.6 cm^{-1} for $^{\bullet}CH_3$, considerably different from the experimental values of 444(13) cm^{-1} (this work) and 606.4531 cm^{-1} (ref 21), respectively. Also, the calculations show an inversion barrier of 720.5 cm^{-1} and suggest that the electron is not bound at planarity; i.e., the electronic potential energy surfaces cross before the D_{3h} geometry is attained. Considering their calculated anion fundamental ν_2 (784 cm^{-1}), the $\nu_2(v'' = 1^+)$ vibrational level would be considerably higher than the neutral ZPE (by 420 cm^{-1}), and therefore, the $\nu_2(v'' = 1^+)$ anion would be unstable with respect to electron autodetachment, a finding that contradicts our observation of this level persisting for at least several milliseconds. Unfortunately, there is no reported calculation of the Δ_{inv} in the most recent work from Dixon et al. to compare with our experimental and calculated values. With the large basis sets including diffuse functions and the high-level treatment of correlation effects used here, we did not experience the issue of electron autodetachment at planarity. Accordingly, our quantum mechanical treatment is entirely adiabatic, an assumption that seems to be borne out by the agreement with experiment. For more details on the anion and neutral potential energy surface crossing with the reported calculations, see the Supporting Information.

6. CONCLUSIONS

In this work, we report the high-resolution gas-phase photoelectron spectra of CH_3^- and CD_3^-, the simplest carbanions. The spectra show an extensive vibrational progression in the ν_2 umbrella mode of the $^{\bullet}CH_3$ and $^{\bullet}CD_3$ radicals, indicating the transition from a pyramidal C_{3v} anion to a planar D_{3h} neutral, confirming previous results reported in the literature. We determine a much more accurate value of 0.093(3) eV for the $^{\bullet}CH_3$ electron affinity, as well as that of $^{\bullet}CD_3$, 0.082(4) eV. With these measured EAs, we determine improved values for 0 K gas-phase acidities of CH_4 and CD_4 as 414.79(6) and 417.58(8) kcal/mol, respectively. With the available high-resolution vibrational spectroscopy data, we are able to report the first experimental determination of the inversion splitting in CH_3^- and CD_3^- as 21(5) and 6(4) cm^{-1}. We also measure the $\nu_2(v'' = 0^+ \rightarrow 1^+)$ frequency in CH_3^- and CD_3^- as 444(13) and 373(12) cm^{-1}, respectively. The calculations reported herein are consistent with the experimental findings to a high degree of accuracy. With this in mind, we report a calculated 1D effective barrier to inversion, E_B^{eff}, of 661 cm^{-1} for CH_3^-. The dependence of the photoelectron angular distribution anisotropy on the photoelectron kinetic energy affirms that the methide anion HOMO arises primarily from sp^3 hybridization. These results provide a benchmark for further theoretical studies of the methide anion. Questions that remain unanswered and require further theoretical treatment of this system include issues associated with a possible anion/neutral electronic potential energy surface crossing in the vicinity of the planar geometry. Successful theoretical treatment of the complexities of the simplest of carbanions opens up the possibility of extending these calculations to more complex carbanions. These results expand the field of carbanion chemistry by adding a detailed study of the simplest carbanion structure and properties.

■ ASSOCIATED CONTENT

Supporting Information

The Supporting Information is available free of charge on the ACS Publications website at DOI: 10.1021/jacs.5b07013.

Details regarding uncertainty in the energy-scale calibration, photoelectron angular distributions and analysis, rotational contour shift of the EA, gas-phase acidities at 298 K, theoretical methods, and a discussion of neutral and anion surface crossing at anion planarity (PDF)

■ AUTHOR INFORMATION

Corresponding Author

*wcl@jila.colorado.edu

Present Address

⊥Y.-J.L.: Intel Corp., 2501 NW 229th Ave., Hillsboro, OR 97124.

Notes

The authors declare no competing financial interest.

■ ACKNOWLEDGMENTS

W.C.L. gratefully acknowledges support from the National Science Foundation (NSF) (Grants PHY1125844 and CHE1213862) and Air Force Office of Scientific Research (AFOSR) (Grant FA9550-12-1-0125) for significant contributions to this project. P.B.C. is supported by NSF Grant DGE1144083. J.F.S. thanks the Robert A. Welch Foundation (Grant F-1283) for support. We thank Prof. G. B. Ellison for helpful discussions.

■ REFERENCES

(1) Peoples, P. R.; Grutzner, J. B. *J. Am. Chem. Soc.* **1980**, *102*, 4709.
(2) Carey, F. A.; Sundberg, R. J. *Advanced Organic Chemistry*; Springer: New York, 2007; p 579.
(3) Breslow, R. *J. Am. Chem. Soc.* **1958**, *80*, 3719.
(4) Squires, R. R. *Acc. Chem. Res.* **1992**, *25*, 461.
(5) Lukeman, M.; Scaiano, J. C. *J. Am. Chem. Soc.* **2005**, *127*, 7698.
(6) Tian, Z.; Kass, S. R. *Chem. Rev.* **2013**, *113*, 6986.
(7) Vuitton, V.; Lavvas, P.; Yelle, R. V.; Galand, M.; Wellbrock, A.; Lewis, G. R.; Coates, A. J.; Wahlund, J. E. *Planet. Space Sci.* **2009**, *57*, 1558.
(8) Capone, L. A.; Whitten, R. C.; Dubach, J.; Prasad, S. S.; Huntress, W. T. *Icarus* **1976**, *28*, 367.
(9) Borucki, W. J.; Levin, Z.; Whitten, R. C.; Keesee, R. G.; Capone, L. A.; Summers, A. L.; Toon, O. B.; Dubach, J. *Icarus* **1987**, *72*, 604.
(10) Coates, A. J.; Crary, F. J.; Lewis, G. R.; Young, D. T.; Waite, J. H.; Sittler, E. C. *Geophys. Res. Lett.* **2007**, *34*, L22103.
(11) Ellison, G. B.; Engelking, P. C.; Lineberger, W. C. *J. Am. Chem. Soc.* **1978**, *100*, 2556.
(12) Tyminska, N.; Wloch, M.; Royappa, A. T. *Int. J. Quantum Chem.* **2015**, *115*, 42.
(13) DePuy, C. H.; Gronert, S.; Barlow, S. E.; Bierbaum, V. M.; Damrauer, R. *J. Am. Chem. Soc.* **1989**, *111*, 1968.
(14) Tian, Z. X.; Chan, B.; Sullivan, M. B.; Radom, L.; Kass, S. R. *Proc. Natl. Acad. Sci. U. S. A.* **2008**, *105*, 7647.

DOI: 10.1021/jacs.5b07013
J. Am. Chem. Soc. 2015, 137, 12939−12945

(15) Graul, S. T.; Squires, R. R. *J. Am. Chem. Soc.* **1989**, *111*, 892.
(16) Mitchell, S. E.; Conklin, P. M.; Farley, J. W. *J. Chem. Phys.* **2003**, *118*, 11017.
(17) Herzberg, G.; Shoosmith, J. *Can. J. Phys.* **1956**, *34*, 523.
(18) Herzberg, G. *Proc. R. Soc. London, Ser. A* **1961**, *262*, 291.
(19) Jacox, M. E. *J. Mol. Spectrosc.* **1977**, *66*, 272.
(20) Dyke, J.; Neville, J.; Lee, E.; Morris, A. *J. Chem. Soc., Faraday Trans. 2* **1976**, *72*, 1385.
(21) Yamada, C.; Hirota, E.; Kawaguchi, K. *J. Chem. Phys.* **1981**, *75*, 5256.
(22) Frye, J. M.; Sears, T. J.; Leitner, D. *J. Chem. Phys.* **1988**, *88*, 5300.
(23) Sears, T. J.; Frye, J. M.; Spirko, V.; Kraemer, W. P. *J. Chem. Phys.* **1989**, *90*, 2125.
(24) Hermann, H. W.; Leone, S. R. *J. Chem. Phys.* **1982**, *76*, 4759.
(25) Schwenke, D. W. *Spectrochim. Acta, Part A* **1999**, *55*, 731.
(26) Zahedi, M.; Harrison, J. A.; Nibler, J. W. *J. Chem. Phys.* **1994**, *100*, 4043.
(27) Davis, S.; Anderson, D. T.; Duxbury, G.; Nesbitt, D. J. *J. Chem. Phys.* **1997**, *107*, 5661.
(28) Fawzy, W. M.; Sears, T. J.; Davies, P. B. *J. Chem. Phys.* **1990**, *92*, 7021.
(29) Miller, J. T.; Burton, K. A.; Weisman, R. B.; Wu, W. X.; Engel, P. S. *Chem. Phys. Lett.* **1989**, *158*, 179.
(30) Kari, R. E.; Csizmadia, I. G. *J. Chem. Phys.* **1969**, *50*, 1443.
(31) Surratt, G. T.; Goddard, W. A., III *Chem. Phys.* **1977**, *23*, 39.
(32) Cleeton, C. E.; Williams, N. H. *Phys. Rev.* **1934**, *45*, 234.
(33) Jones, L. H. *J. Mol. Spectrosc.* **1979**, *74*, 409.
(34) Murzin, S. N.; Stepanov, O. N. *Opt. Spektrosk.* **1990**, *69*, 497.
(35) Gordon, J. P.; Zeiger, H. J.; Townes, C. H. *Phys. Rev.* **1954**, *95*, 282.
(36) Gordon, J. P.; Wang, T. C.; Zeiger, H. J.; Townes, C. H. *Science* **1954**, *120*, 780.
(37) Liu, D. J.; Oka, T. *Phys. Rev. Lett.* **1985**, *54*, 1787.
(38) Sears, T. J.; Bunker, P. R.; Davies, P. B.; Johnson, S. A.; Spirko, V. *J. Chem. Phys.* **1985**, *83*, 2676.
(39) Araki, M.; Ozeki, H.; Saito, S. *J. Chem. Phys.* **1998**, *109*, 5707.
(40) Duke, A. J. *Chem. Phys. Lett.* **1973**, *21*, 275.
(41) Marynick, D. S.; Dixon, D. A. *Proc. Natl. Acad. Sci. U. S. A.* **1977**, *74*, 410.
(42) Dykstra, C. E.; Hereld, M.; Lucchese, R. R.; Schaefer, H. F.; Meyer, W. *J. Chem. Phys.* **1977**, *67*, 4071.
(43) Padgett, A.; Krauss, M. *J. Chem. Phys.* **1960**, *32*, 189.
(44) Dixon, D. A.; Feller, D.; Peterson, K. A. *J. Phys. Chem. A* **1997**, *101*, 9405.
(45) Ortiz, J. V. *J. Am. Chem. Soc.* **1987**, *109*, 5072.
(46) Lee, T. J.; Schaefer, H. F. *J. Chem. Phys.* **1985**, *83*, 1784.
(47) Kraemer, W. P.; Špirko, V.; Malmqvist, P.-A.; Roos, B. O. *J. Mol. Spectrosc.* **1991**, *147*, 526.
(48) Rajamaki, T.; Miani, A.; Halonen, L. *J. Chem. Phys.* **2003**, *118*, 10929.
(49) Sheps, L.; Miller, E. M.; Lineberger, W. C. *J. Chem. Phys.* **2009**, *131*, 064304.
(50) Lu, Y. J.; Lehman, J. H.; Lineberger, W. C. *J. Chem. Phys.* **2015**, *142*, 044201.
(51) Dribinski, V.; Ossadtchi, A.; Mandelshtam, V. A.; Reisler, H. *Rev. Sci. Instrum.* **2002**, *73*, 2634.
(52) Cooper, J.; Zare, R. N. *J. Chem. Phys.* **1968**, *48*, 942.
(53) Mabbs, R.; Grumbling, E. R.; Pichugin, K.; Sanov, A. *Chem. Soc. Rev.* **2009**, *38*, 2169.
(54) Sanov, A. *Annu. Rev. Phys. Chem.* **2014**, *65*, 341.
(55) Sanov, A.; Grumbling, E. R.; Goebbert, D. J.; Culberson, L. M. *J. Chem. Phys.* **2013**, *138*, 054311.
(56) Grumbling, E. R.; Sanov, A. *J. Chem. Phys.* **2011**, *135*, 164302.
(57) Engelking, P. C. *J. Phys. Chem.* **1986**, *90*, 4544.
(58) CFOUR, Coupled-Cluster Techniques for Computational Chemistry, a quantum-chemical program package by J. F. Stanton, J. Gauss, M. E. Harding, and P. G. Szalay, with contributions from A. A. Auer, R. J. Bartlett, U. Benedikt, C. Berger, D. E. Bernholdt, Y. J. Bomble, L. Cheng, O. Christiansen, M. Heckert, O. Heun, C. Huber, T.-C. Jagau, D. Jonsson, J. Jusélius, K. Klein, W. J. Lauderdale, D. A. Matthews, T. Metzroth, L. A. Mück, D. P. O'Neill, D. R. Price, E. Prochnow, C. Puzzarini, K. Ruud, F. Schiffmann, W. Schwalbach, C. Simmons, S. Stopkowicz, A. Tajti, J. Vázquez, F. Wang, and J. D. Watts, and the integral packages MOLECULE (J. Almlöf and P .R. Taylor), PROPS (P. R. Taylor), and ABACUS (T. Helgaker, H. J. Aa. Jensen, P. Jørgensen, and J. Olsen) and ECP routines by A. V. Mitin and C. van Wüllen. For the current version, see http://www.cfour.de.
(59) NITROGEN, Numerical and Iterative Techniques for Rovibronic Energies with General Internal Coordinates, a program written by P. B. Changala. http://www.colorado.edu/nitrogen.
(60) Ruscic, B. *J. Phys. Chem. A* **2015**, *119*, 7810.
(61) Jentschura, U. D.; Kotochigova, S.; LeBigot, E. O.; Mohr, P. J. and Taylor, B. N. *The Energy Levels of Hydrogen and Deuterium (version 2.1)*. Available: http://physics.nist.gov/PhysRefData/HDEL/energies.html. National Institute of Standards and Technology, Gaithersburg, MD, 2015.
(62) Song, Y.; Qian, X. M.; Lau, K. C.; Ng, C. Y. *Chem. Phys. Lett.* **2001**, *347*, 51.
(63) Ervin, K. M.; DeTuri, V. F. *J. Phys. Chem. A* **2002**, *106*, 9947.
(64) Rajamaki, T.; Miani, A.; Halonen, L. *J. Chem. Phys.* **2003**, *118*, 6358.

DOI: 10.1021/jacs.5b07013
J. Am. Chem. Soc. 2015, 137, 12939−12945